INVITED PAPER

A latent crosslinkable PCL-based polyurethane: Synthesis, shape memory, and enzymatic degradation

Wenbin Kuang and Patrick T. Mather[a)]
Syracuse Biomaterials Institute and Biomedical and Chemical Engineering Department, Syracuse University, Syracuse, New York 13244, USA

(Received 11 April 2018; accepted 13 June 2018)

Seeking a latent-crosslinkable, mechanically flexible, fully thermoplastic shape memory polymer, we have developed a simple but effective macromolecular design that includes pendent crosslinking sites via the chain extender of a polyurethane architecture bearing semicrystalline poly(ε-caprolactone) (PCL) soft segments. This new composition was used to prepare fibrous mats by electrospinning and films by solvent casting, each containing thermal initiators for chemical crosslinking. The one-step synthesis strategy proved successful, and the crosslinking sites within PCL segments resulted in two-way (reversible) shape memory: repeatable elongation (cooling) and contraction (heating) under constant tensile stress. Being fully characterized, the crosslinked fiber mats revealed promising one-way and two-way (reversible) shape memory phenomena, with lower storage moduli though, compared to uncrosslinked films. We observed for both fibrous mats and films that increasing the applied tensile stress led to greater crystallization-induced elongation upon cooling as well as smaller strain hysteresis, particularly for covalently crosslinked samples. Relevant to medical applications, the materials were observed to feature unique, two-stage enzymatic degradation that was sensitive to differences in crystallinity and microstructure among samples.

I. INTRODUCTION

Shape memory polymers (SMPs) have attracted a lot of interest, both academically and industrially, based on the ability to set a temporary, nonequilibrium shape until they are triggered to revert to original shape by a specific external stimulus.[1–3] Several environmental stimuli that can trigger shape changing of SMPs have been well studied thus far, such as heat, light, humidity, electric field, magnetic field, and variation of pH. Among the external stimuli, heat is the most widely investigated and used, as a result of the ease in ability to tailor thermomechanical properties of thermally actuated SMPs.[3] Consequently, thermally activated SMPs offer complexity of material response, including multistage shape change behavior[4–6] and reversible (two-way shape memory) actuation.[7,8] Such response complexity can then be manipulated and tuned through variations in material composition, fabrication method, and post-synthesis processes.

A need exists for rapid and reliable reversible actuation in SMPs to make artificial muscles or other actuators.[6,9,10] Addressing this need, liquid crystalline elastomers (LCEs)[11,12] have been shown to exhibit excellent performance, attributed to the coupling of the self-organization of the liquid crystalline phase and the entropy elasticity of polymer networks. In general, when an external stress is applied, LCEs elongate during cooling from the isotropic (amorphous) state to the liquid crystalline phase, and contract during heating by achieving the strain associated with tensile modulus at the isotropic state. Remarkably, "monodomain" samples feature actuation along the orientation axis with no external stress bias.[13] Toward attaining this reversible actuation behavior in a simple synthetic way, researchers have unveiled multiple macromolecular designs beyond LCEs that can also give rise to actuation. In our own lab, Chung et al.[14] reported on tunable two-way shape memory behavior of crosslinked poly(cyclooctene) by variation of peroxide concentrations. In another approach, Baker et al.[15] fabricated porous foams with body temperature triggering shape memory by crosslinking functionalized poly(ε-caprolactone) (PCL) and poly(ethylene gylcol) via thiol–ene chemistry, and, interestingly, the foams revealed reversible actuation behavior in compression other than in tension as commonly investigated. Besides the work accomplished by our own lab, Behl et al.[16] developed a reversible shape memory copolymer network that consists of a poly(ω-pentadecalactone) segment determining the shape-changing geometry and PCL segment providing the thermally activated actuation. Zhou et al.[17] synthesized an end-capped poly(octylene adipate) that showcased both one-way and two-way

a)Address all correspondence to this author.
e-mail: patrick.mather@bucknell.edu
DOI: 10.1557/jmr.2018.220

 © Materials Research Society 2018

https://doi.org/10.1557/jmr.2018.220 Published online by Cambridge University Press

reversible shape memory phenomena after thio crosslinked and acrylate crosslinked by exposing to 365 nm light.

With growing need in biomaterials and environmentally friendly materials, biodegradable PUs have been studied extensively as one of the specialized SMPs in the field of shape memory research. Teramoto et al.[18] elaborated a novel approach that used a multistep copolymerization of L-lactide, ε-caprolactone, and ethylene glycol oligomer to yield a biodegradable, semicrystalline copolymer containing backbone carbon–carbon double bonds. This copolymer could subsequently be crosslinked chemically, enabling the two-way shape memory behavior. Additionally, the compositional selection of diisocyanates and the molecular weight of soft segments have been found to play leading roles in tailoring select thermal, mechanical, and shape memory properties of PUs.[19,20] Beyond composition, material form, and microstructural characteristics of SMPs may impose an equal influence on these properties. Electrospinning, as a highly versatile and widely used technique that allows fabrication of continuous, fine fibers, has been primarily applied on polymers (both synthetic and natural), and even metal alloys and ceramics.[21,22] Demir et al.[23] obtained an electrospun PU based on poly(tetramethylene oxide) and also studied the effect of electric field, surrounding temperature, conductivity, and viscosity of the polymer solution on structural properties of resulting fibers. However, to our best knowledge, no one has yet to combine electrospinning with thermal curing, especially for biodegradable PUs with a relatively low melting temperature.

For the present study, we sought to prepare fine fibers via electrospinning and to then post-cure the fibrous web to achieve two-way shape memory behavior. In this work, the approach we have implemented involves the use of 3,4-dihydroxy-1-butene (DHB), functioning as a chain extender in polyurethane chemistry with a pendant allyl group that, simultaneously, serves to enable crosslinking while controlling the melting transition and crystallinity.[24–26] As variation in T_m near room temperature impacts crystallinity, and therefore shape memory behavior, manipulation thereof offers an effective approach to tune thermomechanical and potentially biological functions as a biomaterial. Our specific goal with current work was to develop crosslinkable, electrospinnable, and biodegradable thermoplastic polyurethanes that feature two-way reversible shape memory behavior while maintaining comparable thermal and mechanical properties after processing and curing. Our approach was first to synthesize linear PCL-based thermoplastic polyurethanes[27] (subsequently referred to as PCL-TPUs) from polycaprolactone-diol, as a short, biodegradable soft segment and DHB, as a crosslinkable unit with a diisocyanate as the segment linker. We next processed the synthesized PUs into both fiber mats (by electrospinning) and films (by solvent casting), each containing initiators for thermal curing, respectively. Thermal, mechanical, and shape memory properties of the crosslinked materials were characterized, to further investigate the effect of processing and curing on these properties. Moreover, based on the knowledge gained from previous work,[28–30] an enzymatic degradation study was conducted to study the degradation behavior and reveal possible mechanisms.

II. EXPERIMENTAL

A. Materials

Poly(caprolactone)-diols (PCL_{2k}, average $M_n \sim$ 2000 g/mol, purchased from Sigma-Aldrich, St. Louis, Missouri; PCL_{3k}, average $M_n \sim$ 3000 g/mol, purchased from Scientific Polymer Products, Inc., Ontario, New York) were vacuum dried for 2 d prior to use. 3,4-dihydroxy-1-butene (DHB, ≥99%), dilauroyl peroxide (DLP; Luperox® LP, 97%), phosphate buffered saline (PBS; dry powder, pH 7.4 containing TWEEN® 20), and sodium azide (ReagentPlus®, ≥99.5%) were purchased from Sigma-Aldrich (St. Louis, Missouri) and used as received. Hexamethylene diisocyanate (HDI, purum, ≥98%) was purchased from Sigma-Aldrich and stored over 3 Å molecular sieves (Sigma-Aldrich, St. Louis, Missouri) for 3 d before further use. The Tin-POMS catalyst was purchased from Hybrid Plastics and vacuum dried extensively for a week prior to use. Lipase from *Pseudomonas cepacia* (powder, light beige, ≥30 U/mg) was purchased from (Sigma-Aldrich, St. Louis, Missouri) and stored in a freezer ($T \sim -20$ °C) before use. Toluene, chloroform, and *n*-hexanes were all purchased from Fisher Scientific (Hampton, New Hampshire). Toluene was dehydrated by refluxing over calcium hydride (Sigma-Aldrich, St. Louis, Missouri) multiple times until collection and stored over 3 Å molecular sieves for 3 d before use. *N*,*N*-Dimethylformamide (DMF, anhydrous, 99.8%), HPLC-grade tetrahydrofuran (THF), and deuterated chloroform (Chloroform-d, 99.8% atom D) were purchased from Sigma-Aldrich (St. Louis, Missouri) and used as received.

B. Polyurethane synthesis

A one-pot synthesis method was adopted to synthesize the PCL-TPUs from PCL-diol, HDI, and DHB, as shown in Fig. 1. A Schlenk line (AF-0452, purchased from Chemglass Life Sciences, Vineland, New Jersey) was utilized to create air-free reaction environment during the course of polymerization. Moisture was removed from the whole reaction system by evacuating and refilling clean nitrogen at least three times. A 500-mL Schlenk flask (AF-0528, single neck, round bottom) was oven-dried at 80 °C and flame-dried right before use. As a representative example, we specify the preparation of

https://doi.org/10.1557/jmr.2018.220 Published online by Cambridge University Press

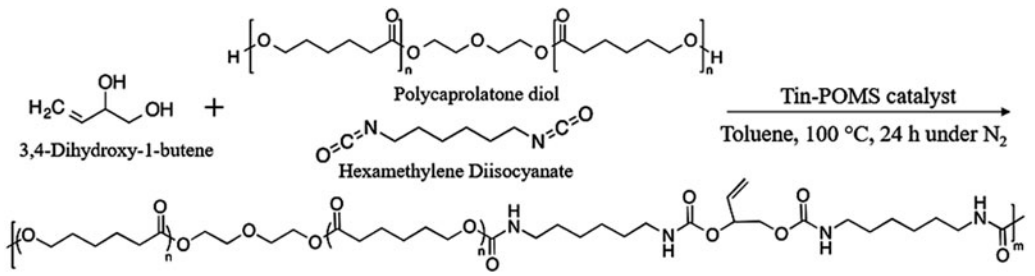


FIG. 1. Preparation of PCL-based thermoplastic polyurethanes (PCL-TPU) by reacting polycaprolactone-diol (PCL-diol) and 3,4-dihydroxy-1-butene (DHB) with hexamethylene diisocyanate (HDI).

PCL_{3k}-TPU as below. A mass of 9.0 g (3.0 mmol) PCL_{3k} was dissolved in 100 mL distilled toluene within a 500-mL flask that was subsequently heated to and kept at 100 °C for about 30 min, while 100 mg (1 wt%) tin-POMS catalyst was dissolved into 5 mL distilled toluene for further use. Once the polymer solution became transparent, indicating that polymer was fully dissolved, 0.18 mL (2.1 mmol) DHB, 0.96 mL (6.0 mmol) HDI, and 5 mL toluene containing Tin-POMS were added into the flask via a syringe under an inert atmosphere of nitrogen. Incubation as such was maintained at 100 °C for 24 h to accomplish polymerization while stirring was kept to assure good mixing. A noticeable increase in viscosity during polymerization was witnessed. Following polymerization as described, the resulting polymer solution was precipitated in a dropwise solution in an 8-fold excess of n-hexane, followed by washing with deionized water. The precipitates were collected and dried in a fume hood overnight prior to complete drying in a vacuum oven at room temperature for another 3 d.

C. Molecular characterization

The PCL_{2k}-TPU and PCL_{3k}-TPU isolated by the method mentioned above were prepared for molecular characterization in deuterated chloroform ($CDCl_3$) at a concentration ranging from 20 to 30 mg/mL. Proton nuclear magnetic resonance (^{1}H NMR) spectra were generated using a Bruker Avance III HD 400 MHz spectrometer (Bruker, Billerica, Massachusetts), to qualitatively verify the chemical structure of synthesis products as well as to quantitatively analyze PCL-to-DHB mol. ratio per chain. The relaxation delay time is 1 s at a temperature of 25 °C. Gel permeation chromatography (GPC) was performed to determine number-average molecular weight (M_w) and polydispersity index (PDI, M_w/M_n), using a Waters Isocratic HPLC system equipped with a temperature-controlled differential refractometer (Waters 2414). Multi-angle laser light scattering (Wyatt miniDAWN, Wyatt, Santa Barbara, California) was introduced at three characteristic angles (45°, 90°, and 135°) for in-line absolute molecular weight determination. The flow rate of THF as the mobile phase in this GPC system was set at 1 mL/h constantly. Polymer-THF solutions (2–5 mg/mL) were passed through a 0.2 μm PTFE filter (Waters, Milford, Massachusetts) prior to injection at 40 °C.

D. Sample preparation

Seeking to understand the effect of PCL_{3k}-TPU before and after processing and curing on thermal, mechanical, and shape memory properties, as-synthesized polymers were processed into films, by solvent casting, and, fiber mats, by electrospinning. To make films, 2 g PCL_{3k}-TPU and 40 mg (2 wt%) DLP were dissolved together into 20 mL chloroform, and the solutions then incubated in an Excella shaker (Excella E24, New Brunswick Scientific, Edison, New Jersey) at 37 °C until becoming completely transparent and homogeneous. The uniform solutions were then cast into a 12.7 cm Teflon dish upon a large, level platen, and allowed to dry for 48 h. Cast films were further dried under vacuum (20 mmHg). To prepare electrospun fiber mats, a 17% (w/v) PCL_{3k}-TPU solution was prepared by adding 2 g PCL_{3k}-TPU and 40 mg DLP into a mixture of 8 mL chloroform and 4 mL DMF. The resulting solution was then heated to and kept at 37 °C with constant stirring. After dissolution completion, each polymer solution was processed into a nonwoven fibrous web (thickness ~0.15 mm) using a custom electrospinning set-up that has been previously reported by our group.[31] The ejecting needle was held at a potential of 16 kV, the tip-to-collector distance was 10 cm, and the rotation rate of a 57.1 mm collecting mandrel was maintained at 400 rpm while the drum was held at a potential of negative 0.5 kV and a flow rate of polymer solution supplying the 22 gauge needle was 1.5 mL/h, all used over the 8 h electrospinning process. Complete drying of spun fiber mats was subsequently achieved in a vacuum oven at room temperature (20 mm Hg) before further use.

Dried films and fibrous webs were cured thermally by the following method. The samples (~2 g) were sandwiched between two polished stainless steel sheets coated with the mold release agent (Pol-Ease® 2300, Polytek, Elizabeth, New Jersey), and a 0.15 mm thick stainless steel spacer was placed in between to control the thickness of the final film. A 0.25 MPa compressive

https://doi.org/10.1557/jmr.2018.220 Published online by Cambridge University Press

stress and a customized ramping heating method (temperature was set at 60 °C initially, ramping up to 90 °C by 20 °C/h, and finally kept at 90 °C for 30 min) were implemented throughout entire 2 h of curing, using a Carver 3851-0 press with heating platens. Afterward, the platens were cooled down to room temperature at a rate of approximately 30 °C/h, following which the compressive pressure was released.

E. Gel fraction measurement

To assess the extent of covalent crosslinking, network gel fraction values of the crosslinked films and crosslinked fiber mats were examined using a combination of solvent-extraction and gravimetry. Each sample was weighed for its dry mass before being soaked in 20 mL THF at 37 °C in an Excella shaker (New Brunswick Scientific, Elizabeth, New Jersey) for 48 h, during which the THF was refreshed every 12 h. Then, the samples were washed with deionized water, blotted with common towel, and vacuum-dried for a week at room temperature to remove any residual solvent or water. The final dry mass was recorded for calculation of gel fraction. Calculation of gel fraction values involves the initial dry mass, m_i, and the final dry mass, m_f, using the following equation:

$$G(\%) = \frac{m_f}{m_i} \times 100 \quad . \tag{1}$$

Characterized in this way, G may adopt values ranging from 0% for a totally soluble polymer (with no network formation) up to 100% for a perfectly crosslinked network within which no free linear polymer chains exist.

F. Microstructural characterization

To visualize surface morphology and structural geometry of cast films and electrospun fiber mats of PCL_{3k}-TPU, scanning electron microscopy (SEM) was conducted using a JEOL JSM-5600 microscope (JEOL Ltd., Tokyo, Japan) under an accelerating voltage of 5 kV. Both the samples were gold-sputtered for 60 s prior to imaging by using a Fujifilm FLA7000 reader (Tokyo, Japan). Also, to ascertain the molecular ordering and crystalline microstructure, wide-angle X-ray scattering (WAXS) analysis was performed using a Rigaku S-MAX3000 (Auburn Hills, Michigan) for virgin cast films, crosslinked cast films, virgin electrospun fiber mats, and crosslinked electrospun fiber mats of PCL_{3k}-TPUs. A Rigaku MicroMax-002+ generator (Auburn Hills, Michigan) was operated under an accelerating voltage of 45 kV and a current of 0.88 mA to yield a collimated beam of Cu K_α X-rays with a wave length of 1.5405 Å. Scattering patterns were collected (see below) for 30 min except the virgin fiber mat for 15 min due to high transmittance to X-rays. The sample-detector distance was fixed at 120.7 mm, leading to scattering angles $3° < 2\theta < 40°$. WAXS images were obtained and analyzed using a FujiFilm FLA7000 reader (with Fujifilm image plates CR HR-V; Fujifilm, Tokyo, Japan) and SAXSgui software v2.03.04 (JJ X-Ray, Hoersholm, Denmark).

G. Thermal and dynamic mechanical analysis

Differential scanning calorimetry (DSC) was used to investigate thermal properties of all the samples using the TA Instruments Q200 apparatus. Samples weighing approximately 5 mg underwent a thermal program of first heating to 140 °C at 10 °C/min, cooling to −60 °C at 10 °C/min, and then reheating at 10 °C/min to 140 °C while heat flow data were recorded. The melting transition temperature (T_m, the peak of the endotherm), crystallization transition temperature (T_c, the peak of the exotherm), and the enthalpy of melting (ΔH, area beneath endothermic peak) were recorded, respectively, on the basis of the second heating curve (to minimize the effects of thermal history). Crystallinity of PCL_{3k}-TPU was determined using the latent heat of melting relative to an experimentally tested value for fully crystallized PCL_{3k}, using the equation

$$X_c(\%) = \frac{\Delta H_{PCL_{3k}}}{\Delta H_{o,PCL_{3k}}} \times 100 \quad , \tag{2}$$

where $\Delta H_{o,PCL_{3k}}$ is 64.92 J/g. We recognize that this is a rough estimation since the latent heat for TPUs that are fully crystallized will be diluted by noncrystallizable portions of the TPU chains. Thus, only trends in X_c were given attention, not absolute values.

A TA Instruments Q800 dynamic mechanical analyzer (DMA; TA Instruments, New Castle, Delaware) was adopted to explore the thermomechanical properties and also to assess success of crosslinking PCL_{3k}-TPUs (i.e., crosslinked cast film and crosslinked spun fiber mat). In the multifrequency controlled-strain mode, tensile specimens were equilibrated at −60 °C, held isothermal for 10 min, and heated continuously up to 100 °C at 3 °C/min. An oscillating frequency of 1 Hz, an amplitude of approximately 15 μm, a preload force of 0.001 N, and a force track of 108% were utilized. The tensile specimens featured an approximate length-to-width ratio of 4:1 and thicknesses ranging from 0.12 to 0.16 mm.

H. Shape memory characterization

To probe and analyze one-way and two-way (reversible) shape memory behaviors, dog bone-shaped samples (ASTM D63 Type IV, scaled down by a factor of 4) were tested for crosslinked PCL_{3k}-TPUs only, using DMA in the controlled force mode. For one-way shape memory tests, the samples were first strained to 40% at 90 °C, cooled at 2 °C/min to −30 °C under constant tension, released of their tensile stress, and finally heated up to

https://doi.org/10.1557/jmr.2018.220 Published online by Cambridge University Press

90 °C at 2 °C/min. This program was repeated three times for each sample. To quantify the one-way shape memory behavior, the calculation of the shape fixing (R_f) and shape recovery (R_r) ratios[32] for each individual cycle were performed using the equations below:

$$R_f(\%) = \frac{\varepsilon_f - \varepsilon_i}{\varepsilon_d - \varepsilon_i} \times 100 \quad , \tag{3}$$

$$R_r(\%) = \frac{\varepsilon_f - \varepsilon_r}{\varepsilon_f - \varepsilon_i} \times 100 \quad , \tag{4}$$

Here, ε_f stands for the fixed strain after release stress, ε_i stands for the initial strain at starting point of each cycle, ε_d stands for the deformed strain before unloading, and ε_r stands for the recovered strain after complete heating.

By contrast, two-way shape memory tests were performed in the following procedures: at first, each sample was deformed by ramping the applied tensile load at 0.01 N/min to 40% strain at a prescribed elevated temperature. The stress required to achieve this strain was then held fixed for all subsequent steps. Next, the samples were cooled to a prescribed low temperature at 2 °C/min. Finally, and after being held isothermally for 10 min, each sample was reheated to the initial elevated temperature at 2 °C/min. The strains were recorded as a function of temperatures while the heating and cooling steps were done three times in succession. The characteristics associated with two-way shape memory behavior were subsequently evaluated by calculating the actuation magnitude ($R_{a,m}$) and the recovery magnitude ($R_{r,m}$),[14] using the equations as follows:

$$R_{a,m}(\%) = \left(\varepsilon_{low} - \varepsilon_{high}\right) \times 100 \quad , \tag{5}$$

$$R_{r,m}(\%) = \frac{\varepsilon_{low} - \varepsilon_{high}^{final}}{\varepsilon_{low} - \varepsilon_{high}^{initial}} \times 100 \quad , \tag{6}$$

where ε_{low} and ε_{high} are the strains, respectively, at low and high temperatures under loading, $\varepsilon_{high}^{final}$ is the final strain at high temperature with stress applied after recovery, and $\varepsilon_{high}^{initial}$ is the initial strain under stress at high temperature. In addition, the magnitude of hysteresis for each sample was determined as the temperature difference between the 50% actuation strain upon heating (higher temperature) and cooling (lower temperature), averaged for three heating-and-cooling loops generated at the same level of stress. We note that this value is heating/cooling rate dependent[33]; however, exploration of this dependence was beyond the scope of the present work.

I. Enzymatic degradation study

In vitro enzymatic degradation experiments were conducted at 37 °C in a PBS aqueous solution that contains 0.4 mg/mL[34] lipase from *Pseudomonas cepacia*. Sodium azide was added to the PBS buffer at a concentration of 1 mg/mL, to suppress microorganism growth. Virgin cast films, crosslinked cast films, virgin spun fiber mats, and crosslinked spun fiber mats were cut into 10 mm squares with average thicknesses of 0.14, 0.12, 0.06, and 0.03 mm, respectively. Each sample was individually put into 20 mL vials with 5 mL PBS buffer prepared as above. The buffer was replaced with a fresh one every 4 d so as to sustain enzyme activity. At predetermined degradation time points, three samples from each composition were taken out of the PBS buffer, rinsed with deionized water, blotted dry, further dried under vacuum for 4 d at room temperature, and finally weighed. The percentage of mass remaining (which can vary from 100 to 0 over the course of degradation) was calculated using the relation

$$\text{Mass Remaining}(\%) = \left(\frac{M_f}{M_i}\right) \times 100 \quad , \tag{7}$$

wherein M_f is the final dry weight and M_i is the initial dry weight of each sample. The average value of three samples at the same time point is reported for each composition and form, error bars indicating one standard deviation. In addition, crystallinity changes during degradation were monitored using calorimetry [Eq. (2)], with an exception that the amorphous phase of the materials would be more susceptible than the crystalline phases to enzymatic degradation. To further study degradation, perhaps revealing the active mechanism, GPC (M_w and PDI measurements) experiments were applied to uncrosslinked PCL_{3k}-TPU samples while gel fraction measurements [Eq. (1)] were used during degradation to crosslinked PCL_{3k}-TPU samples.

III. RESULTS AND DISCUSSION

A. Molecular characterization

Polyurethanes with varying soft segments were synthesized by condensation polymerization for both PCL_{2k}-diol and PCL_{3k}-diol with DHB and HDI in the presence of the Tin-POMS catalyst (Fig. 1). Through a trial-and-error method (of varying the feed molar ratio), the optimal feed molar ratio of the three reagents was determined to be 3:2.1:6 to maximize yield and molecular weight of the resulting products. The excess of HDI in this molar ratio was used to compensate for possible broad distribution of the PCL molecular weights[35,36] and also for the side reactions with trace water.[37] The results of the polyurethane syntheses are summarized in Table I. ^{1}H NMR spectra confirmed the success of incorporating unsaturation in both PCL_{2k}-TPU and PCL_{3k}-TPU in accordance with characteristic peaks at specific chemical shifts and also revealed that the actual DHB incorporation levels were about 6 and 9.4 mol%, respectively.

https://doi.org/10.1557/jmr.2018.220 Published online by Cambridge University Press

TABLE I. Synthesis summary of PCL-based thermoplastic polyurethanes.

Samples[a] ($n \geq 5$)	Feed molar PCL_{xk}:DHB:HDI[b]	Actual molar PCL_{xk}:DHB[c]	Yield (mass%)	M_w (kDa)	PDI	T_m (°C)[d]	ΔH_m (J/g)
PCL_{2k}-TPU	3:2.1:6	15.58:1	89.3 ± 8.1	288 ± 43.7	2.00 ± 0.28	30.8 ± 1.6	30.4 ± 3.5
PCL_{3k}-TPU	3:2.1:6	9.61:1	90.9 ± 9.3	150.5 ± 38.6	1.79 ± 0.14	45.2 ± 2.6	42.1 ± 1.9

[a]Nomenclature: PCL_{xk} stands for polycaprolactone-diol with Mn = **x** kDa, DHB stands for 3,4-dihydroxy-1-butene, and HDI stands for hexamethylene dissocyanate.
[b]Tuned ratio by trial-and-error method.
[c]Determined by NMR spectra.
[d]Peak values of second heating in the DSC curve.

Moreover, the incorporation of pendant allyl groups resulted in an average 19 or 10 °C drop of melting temperature for PCL_{2k}-TPUs (~31 °C) or PCL_{3k}-TPUs (~45 °C) compared to the melting temperature of their corresponding precursor, either PCL_{2k}-diol (50 °C) or PCL_{3k}-diol (55 °C) (See the Supplementary Material, Fig. S1). Increasing the molecular weight of soft segment correspondingly increased the enthalpy of melting, a direct indicator of crystallinity degree. We chose to use PCL_{3k}-TPUs for following experiments and more detailed investigation because high crystallinity might adversely influence the shape memory effect of polyurethanes[38,39] and relatively low melting temperature that sits around room temperature would possibly cause poor shape fixing so that no good shape memory behavior would be expected if in practical use.

B. Microstructural characterization

SEM images of all PCL_{3k}-TPU samples described in Sec. II.D, compiled in Fig. 2, reveal the surface morphology and internal, cross-sectional structure of different forms of this polymer. Figures 2(a) and 2(e) show that a homogeneously distributed film with smooth surfaces was made using our customized compression molding method. The as-spun fiber mat was imaged at different magnifications, as shown in Figs. 2(b) and 2(f), indicating a capacity of this polymer to easily be processed into a fibrous structure with submicron fiber diameter. Interestingly, the adopted thermal curing process only caused partial melting of the spun fibers, resulting in a structural combination of fiber and matrix composed of a single polymer [Figs. 2(c) and 2(g)]. The crosslinked spun fiber mat was freeze-fractured to allow SEM imaging of the internal structure viewed in cross section. Such views at different magnifications supported the assertion of a fiber–matrix composite structure, as we observed some continuous phases connecting to or wrapping around the fibrous structure clearly in Figs. 2(d) and 2(h). Evidently, part of PCL_{3k}-TPU spun fibers preserved their original fibrous configuration and kept their permanent shapes in that way instead of fully melting to form a uniform film during our customized thermal curing process. The coexistence of fiber and matrix, both made from the same polymer, also fits in the concept of single polymer composite.[40,41] This unique, porous structure could lead to some attractive mechanical and biological properties for broader range of applications.

To further characterize the microstructure of PCL_{3k}-TPU, WAXS experiments were conducted on all four samples, revealing the independence of the crystalline structure on processing or curing. All four samples exhibited a nearly identical WAXS pattern [Figs. 3(a)–3(d)] and thus quite similar trend plots of intensity-versus-2θ [Fig. 3(e)]. Out of all the WAXS patterns, the peak intensities observed for virgin (uncrosslinked) spun fiber mat were relatively sharper than the other three samples, large crystal size. In particular, the soft segment, PCL_{3k}, exhibited two characteristic peaks [Fig. 3(e)] at $2\theta = 21.42°$ and 23.66°, respectively, within a broad range spanning $2\theta = 18.80°$–26.60°. These two peaks relate to *d*-spacings of 4.12 and 3.77 Å. Based on literature reports, the sharp peak at $2\theta = 21.42°$ (4.12 Å) corresponds specifically to the (110)[42] of the PCL crystalline structure.

C. Thermal and dynamic mechanical analysis

Thermal analyses were carried out for virgin cast film, crosslinked cast film, virgin spun fiber mat, and crosslinked spun fiber mat using DSC (See the Supplementary Material, Table SI). First cooling and second heating curves are shown in Fig. 4 for these samples. In general, samples in different forms have been found to have nearly identical T_m's at around 46 °C, indicating no noticeable impact of crosslinking and form on the melting transition. By contrast, T_c's of spun fiber mats slightly shifted to lower temperatures, possibly an artifact attributed to the fibrous microstructure decreasing thermal conductivity. A similar trend was found for enthalpies of melting. The enthalpy of melting for each sample provides an estimate of the crystallinity degree. Thus, our results indicated that the fibrous microstructure decreased crystallinity of the soft segments to some extent, while a higher crosslinking degree decreased crystallinity even further.[43] The latter observation is supported by gel fraction results. The gel fraction value for the crosslinked film was 80% while that for the crosslinked fiber mat was 90%. Given that the same curing condition was applied

https://doi.org/10.1557/jmr.2018.220 Published online by Cambridge University Press

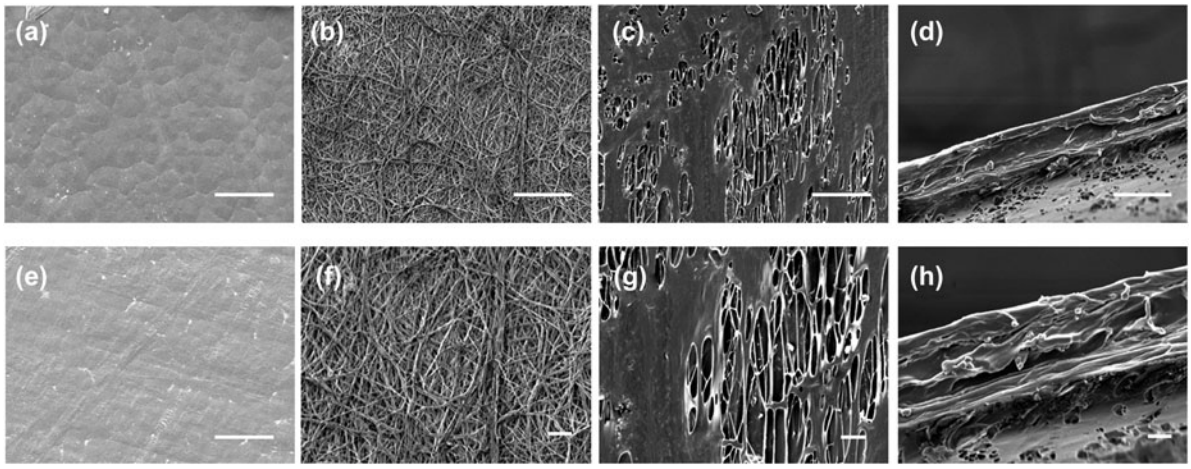


FIG. 2. SEM images of PCL_{3k}-TPU: (a) virgin cast film surface; (e) crosslinked cast film surface; (b) and (f) virgin spun fiber mat surface (770 nm average diameter) at different magnifications; (c) and (g) crosslinked spun fiber mat at different magnifications; (d) and (h) cryofracture (cross section) views of crosslinked spun fiber mat at different magnifications.

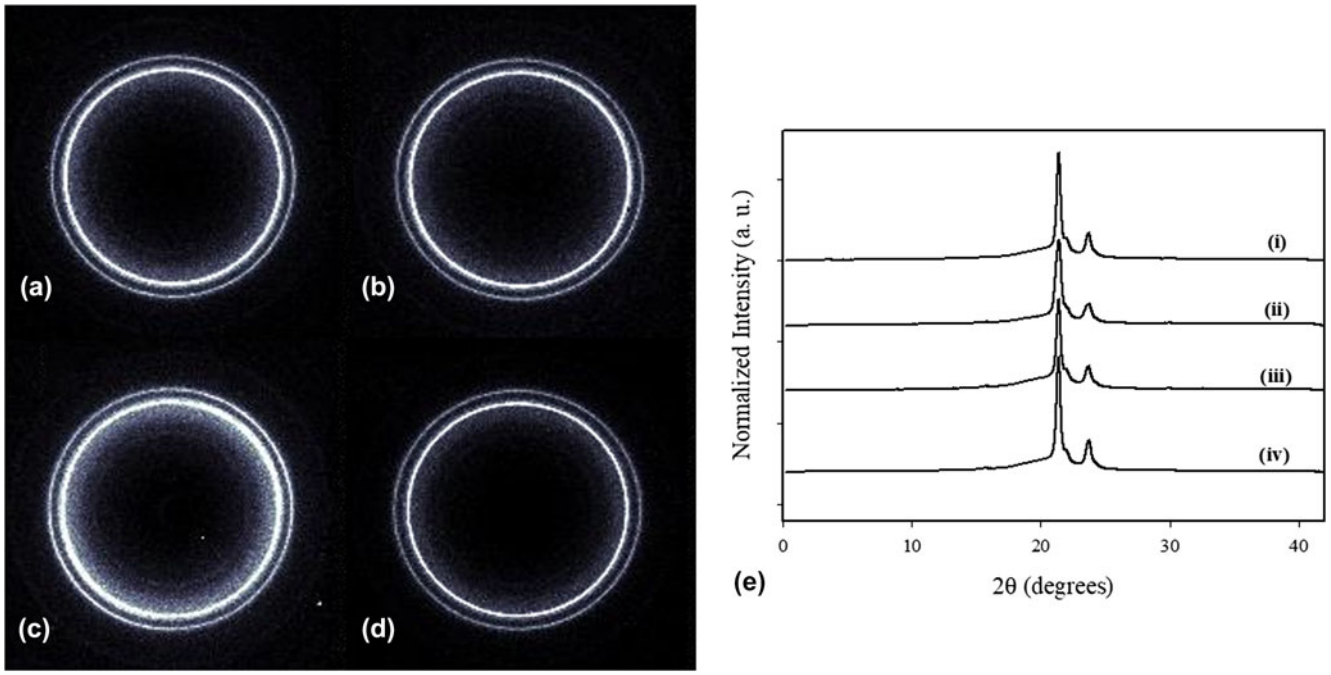


FIG. 3. 2D WAXS patterns of (a) virgin cast film, (b) crosslinked cast film, (c) virgin spun fiber mat, and (d) crosslinked spun fiber mat of PCL_{3k}-TPU; (e) WAXS profiles of (i) virgin cast film, (ii) crosslinked cast film, (iii) virgin spun fiber mat, and (iv) crosslinked spun fiber mat. The X-ray wave length (λ) is 1.5405 Å.

for both samples, the relatively high gel fraction value for the crosslinked fiber mat implies that the electrospinning process resulted in better mixing between the polymer and the crosslinker than solvent casting did.

The results of dynamic mechanical analysis (DMA) are compiled in Fig. 5(a), for films and in Fig. 6(a), for fiber mats, respectively. The temperature-dependent storage modulus was measured to investigate and compare their thermomechanical properties over temperature range spanning −60 to 100 °C. The storage modulus for each sample similarly dropped an order of magnitude upon increasing the temperature from −60 to 20 °C prior to melting transition. Either films or fiber mats softened starting at around 37 °C, as the storage modulus began drop quickly. Both virgin sample mats became too fluid to bear any stress just above 50 °C and finally yielded, as a result of complete melting of the crystalline domain. On the contrary, both crosslinked samples were able to maintain stable rubbery states above their T_m's. Beyond melting, the storage modulus for the crosslinked film leveled out at 1.49 MPa, which was about 3 times higher than the crosslinked fiber mat (~0.50 MPa). We attribute

https://doi.org/10.1557/jmr.2018.220 Published online by Cambridge University Press

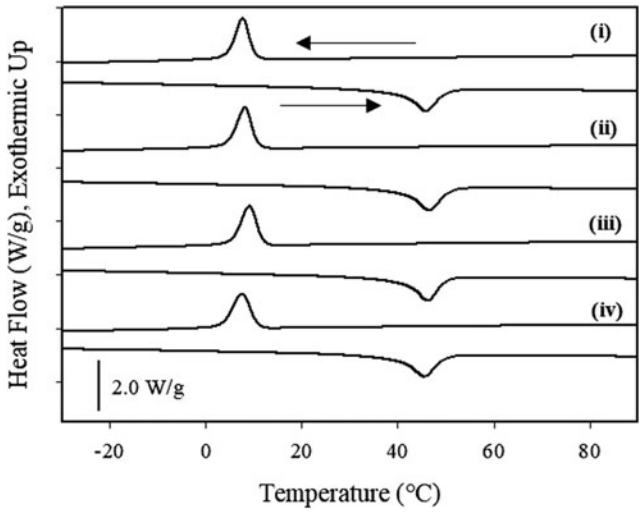


FIG. 4. DSC analysis graph of virgin cast film (i), crosslinked cast film (ii), virgin spun fiber mat (iii), and crosslinked spun fiber mat (iv) of PCL_{3k}-TPU. Heating and cooling rates of 10 °C/min. Arrows suggest heating/cooling directions.

this significant difference to the large fraction of void space existing in the crosslinked spun fiber mat, with the support of prior SEM imaging data. The relative crosslink density can be estimated for comparison purposes by computing the inverse ratio of the modulus in the rubber region to the absolute temperature at which the modulus was measured ($\zeta = T/E'$), ζ being inversely proportional to crosslink density.[44,45] Our results indicate that the crosslinked cast film ($\zeta \sim 2.24 \times 10^{-4}$ K/Pa at 60 °C) has a relatively high crosslink density (low ζ) when compared to the crosslinked electrospun fiber mat ($\zeta \sim 6.85 \times 10^{-4}$ K/Pa at 60 °C), which is not surprising, given the porosity of the latter.

D. Shape memory characterization

In light of previous work[13,46] from our group, the presence of a stable rubbery plateau above T_m should allow such polymeric samples to be deformed extensively and reversibly without macroscopic flow, a prerequisite for a shape memory. Hence, we should expect shape memory behavior for crosslinked samples only, in light of the DMA results discussed in Sec. III.C. The results of one-way shape memory cycles are plotted in three-dimensional stress-temperature-strain graphs [Fig. 5(b) for the crosslinked film and Fig. 6(b) for the crosslinked fiber mat], showing the response of the samples to shape fixing and recovery. Quantification of one-way shape memory behavior involved calculation of fixing and recovery ratios using Eqs. (3) and (4), and the results are summarized in Table II. We observed that both types of crosslinked samples exhibited excellent fixing and recovery ratios, all above 99%, indicating the exceptional capacity of this material to sustain programmed deformation upon loading as well as to recover precisely back to original shape. Furthermore, due to the remarkable increase in strain that occurred during crystallization of PCL_{3k}-bearing TPUs upon cooling [See Figs. 5(b) and 6(b)], it was expected that the crosslinked PCL_{3k}-TPUs would be good candidates for two-way reversible shape memory phenomenon, described next.

Two-way shape memory behavior features reversible elongation and contraction, under constant (or no) loading, upon cooling and heating through the melting transition, respectively. Two-way shape memory cycles for the new materials are shown in Fig. 5(c), for the crosslinked film and in Fig. 6(c), for the crosslinked fiber mat, revealing great potential to change in shape reversibly without noticeable creeps. More interestingly, in both cases, the strain barely changes or slightly increases with decreasing temperature, except during the crystallization where the strain spikes up drastically with an actuation magnitude, $R_{a,m} \sim 15\%$, for the crosslinked film and ~24%, for the crosslinked fiber mat, respectively. The crosslinked fiber mat exhibited a higher actuation magnitude possibly because of its lower storage moduli above T_m. On the other hand, it was observed that the recovery magnitude of the crosslinked film was approximately 10% higher than that of the crosslinked fiber mat. We speculate that there are primarily two factors playing significant roles in affecting recovery magnitude, one being the highly porous structure that may feature fiber-level reconfiguration that is irreversible, the other being the relaxation of residual stresses imparted during the electrospinning and compression molding process. The latter speculation is favorably supported by two-way shape memory cycles of the crosslinked fiber mat [Fig. 6(c)], as we found a relatively low recovery magnitude particularly for the first cycle (~77%).

The estimation of a critical stress,[2,13] σ_c, beyond which stress-induced crystallization occurs is of great importance for consideration as actuators. For materials with $\sigma_c \sim 0$, no applied stress (or stress bias) is needed for finite actuation to occur. It is also known that increasing of applied stress should lead to increasing actuation strain.[13] Therefore, two-way shape memory cycles at different stress levels were performed on the crosslinked film [Fig. 5(d)] and crosslinked fiber mat [Fig. 6(d)]. From such testing, the mean maximum strain increment and mean strain hysteresis were collected and plotted as a function of the stress applied (Fig. 7). We observed that the strain increment of the crosslinked film was elevated from 27.3% up to 42.7% (a 56.4% increase) by increasing the tensile stress from 0.30 to 0.70 MPa (a 133% increase) correspondingly. In comparison, the crosslinked fiber mat revealed a 411% increase of the strain increment from 12.3 to 62.9%, as the stress increased from 0.15 to 0.45 MPa (a 200% increase). Figures 7(a) and 7(b) were then used to calculate critical stress by extrapolating the actuation strain linearly to the

https://doi.org/10.1557/jmr.2018.220 Published online by Cambridge University Press

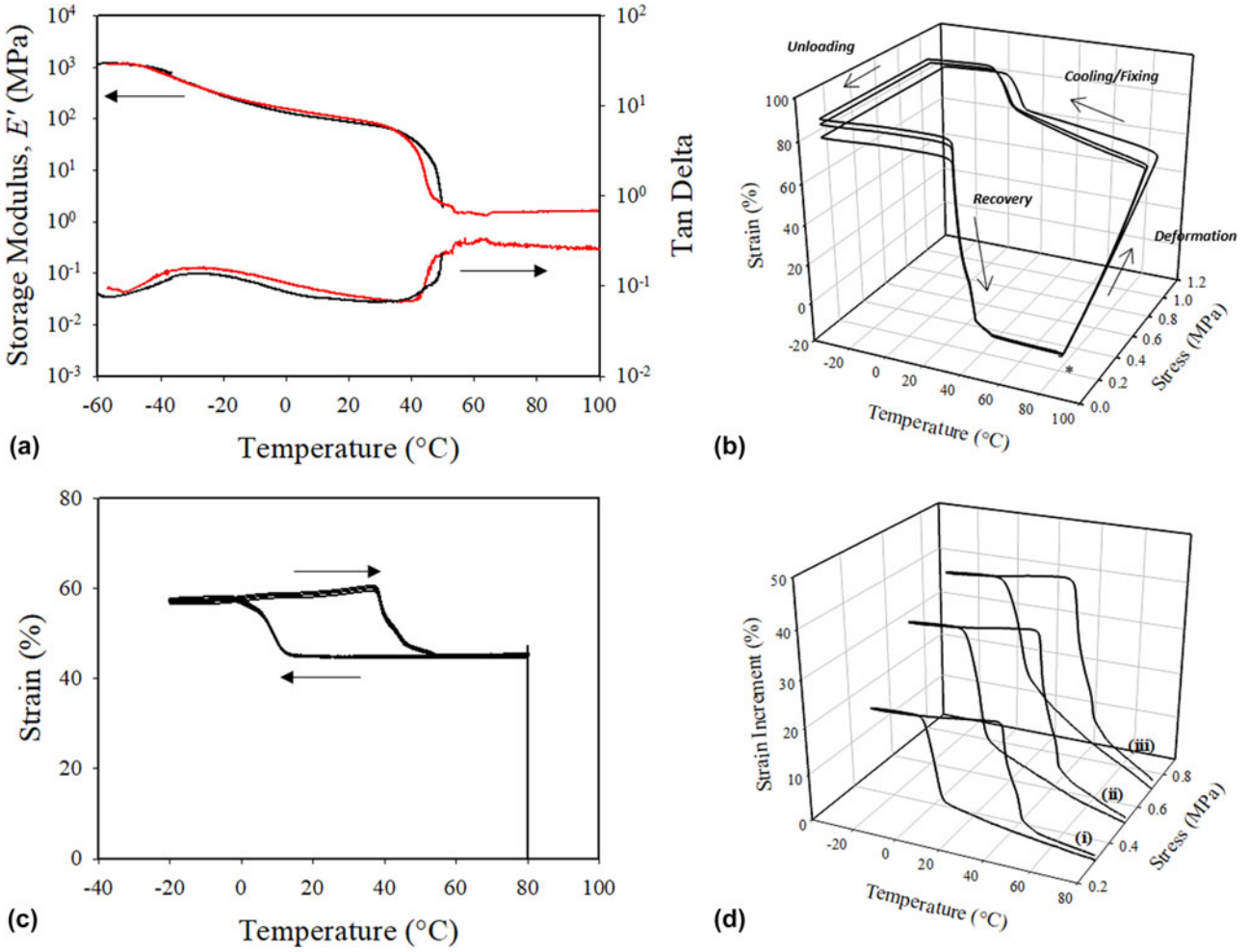


FIG. 5. (a) Storage modulus (E') versus temperatures for the virgin cast film (black) and the crosslinked cast film (red) of PCL_{3k}-TPU. E' was recorded at a heating rate of 3 °C/min with a frequency of 1 Hz; (b) one-way and (c) two-way shape memory cycles for the crosslinked cast film of PCL_{3k}-TPU. "*" indicates the starting point; (d) two-way shape memory behavior for the crosslinked cast film of PCL_{3k}-TPU at different stresses, (i) 0.30 MPa, (ii) 0.50 Mpa, and (iii) 0.70 Mpa. The samples were deformed under each constant stress at 80 °C, followed by cooling and heating steps (2 °C/min), respectively.

stress axis, revealing a $\sigma_c = -0.28$ MPa, for the crosslinked film and a $\sigma_c = 0.08$ MPa, for the crosslinked fiber mat, respectively. Given the fact that crystallization-induced elongation is always inactivated below critical stress, these low critical stress values implied that, theoretically, the external stress would be minimal for this elongation to occur. That said, Fig. 7 also reveals that finite stress is needed for actuation of any practical use.

E. Enzymatic degradation study

For tissue engineering, medical device and drug delivery applications, controlled biodegradation properties are often requirements for the polymeric biomaterials involved. Enzymatic degradation studies, a common method by which the biodegradation rate could be measured rapidly in a short amount of time, have played an important role in characterizing the polymeric materials. In this work, we found a two-step, bulk degradation for the new PCL_{3k}-TPUs, dependent on their crystalline structure and their crosslinking state. Figure 8(a) shows the results of enzymatic degradation profiles of all four types of PCL_{3k}-TPU samples, including virgin cast film, crosslinked cast film, virgin spun fiber mat, and crosslinked spun fiber mat. In general, we found that all the samples experienced a two-stage degradation [Fig. 8(a)]: at the first stage, a much faster degradation phenomenon was found roughly over first two weeks, and at the second stage, the degradation slowed down to the same rate for all the samples through the rest of our experimental time range. To further interpret this special degradation behavior, thermal analysis was done for all the samples at different time points using DSC. The change in crystallinity for each sample was monitored individually over time during the entire degradation study, as shown in Fig. 8(b). As for the virgin fiber mat, no data were recorded after day 22 due to

https://doi.org/10.1557/jmr.2018.220 Published online by Cambridge University Press

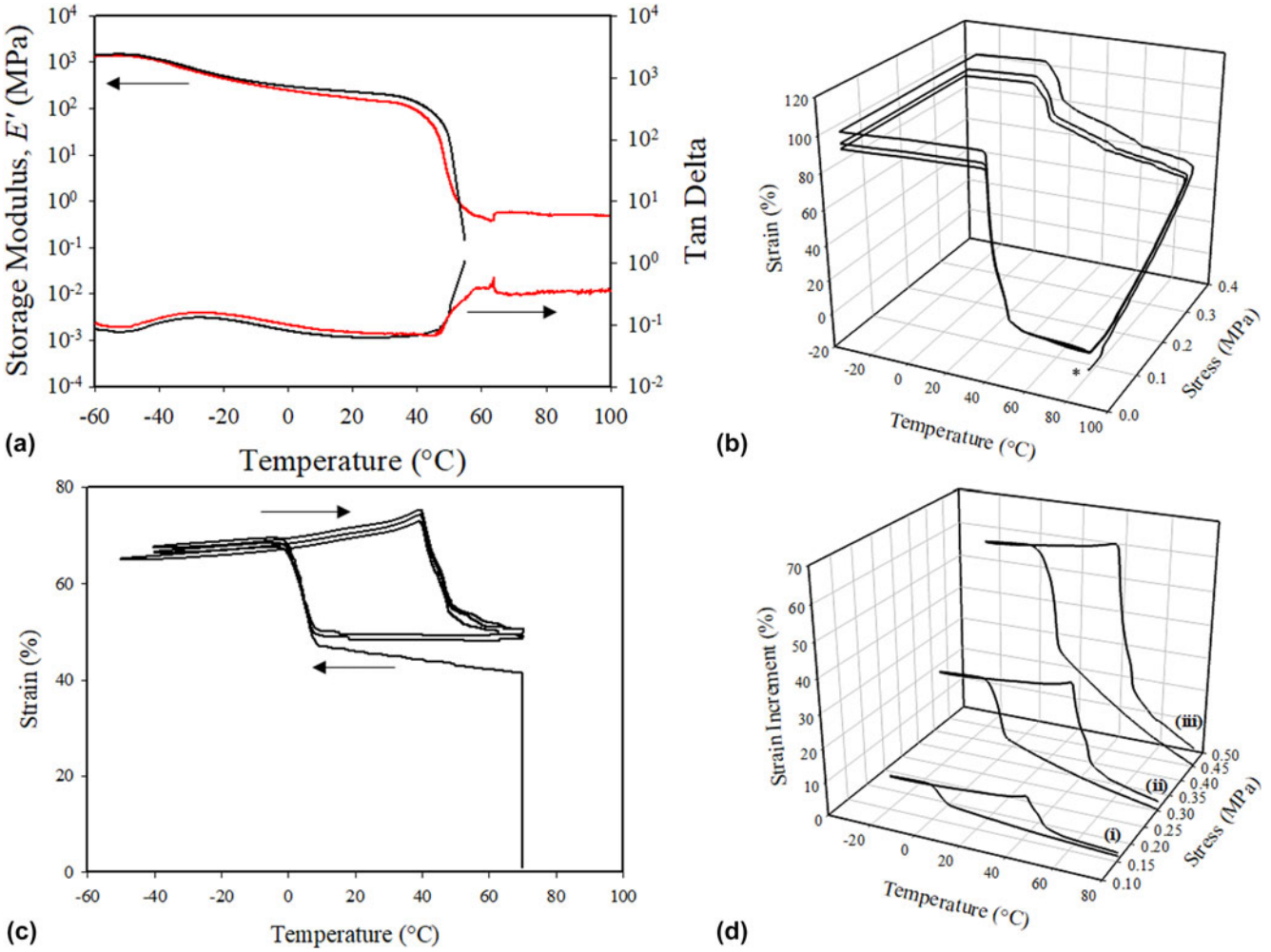


FIG. 6. (a) Storage modulus (E') versus temperatures for the virgin spun fiber mat (black) and the crosslinked spun fiber mat (red) of PCL_{3k}-TPU. E' was recorded at a heating rate of 3 °C/min with a frequency of 1 Hz; (b) one-way and (c) two-way shape memory cycles for the crosslinked spun fiber mat of PCL_{3k}-TPU. "*" indicates the starting point; (d) two-way shape memory behavior for the crosslinked spun fiber mat of PCL_{3k}-TPU at different stresses, (i) 0.15 MPa, (ii) 0.30 Mpa, and (iii) 0.45 Mpa. The samples were deformed under each constant stress at 80 °C, followed by cooling and heating steps (2 °C/min), respectively.

TABLE II. 1WSM and 2WSM characteristics for crosslinked PCL_{3k}-TPUs in different forms.

Sample	R_f (%)	R_r (%)	$R_{a,m}$ (%)	$R_{r,m}$ (%)
Crosslinked cast film	99.34 ± 0.01	99.04 ± 0.42	14.88 ± 0.33	96.90 ± 1.64
Crosslinked spun fiber mat	99.66 ± 0.02	99.48 ± 0.37	23.55 ± 0.64	87.93 ± 8.13

insufficient residual mass, which is beyond capability of our DSC. Then, except for this case, it was clearly observed that the crystallinities of the virgin film, crosslinked film, and crosslinked fiber mat increased to varying degrees with degradation time. Interestingly, crystallinity was observed to increase during early stage of degradation, followed by a leveling off that coincided with the observed degradation profiles. This observation can be understood by considering the fact that the enzymes would preferentially attack the amorphous phase since that amorphous phase is in much lower order than the crystalline region.[34] Accordingly, the amorphous region was broken down at a higher rate, initially, resulting in a relatively fast degradation as well as a quick increase of crystallinity on a percentage basis. Consequently, at this point, the crystallinity at the surface or internal surfaces may be lower than regions at the interior of the sample. However, as degradation proceeded, domains that were more crystalline were exposed to the buffer solution containing the lipases, which in return

https://doi.org/10.1557/jmr.2018.220 Published online by Cambridge University Press

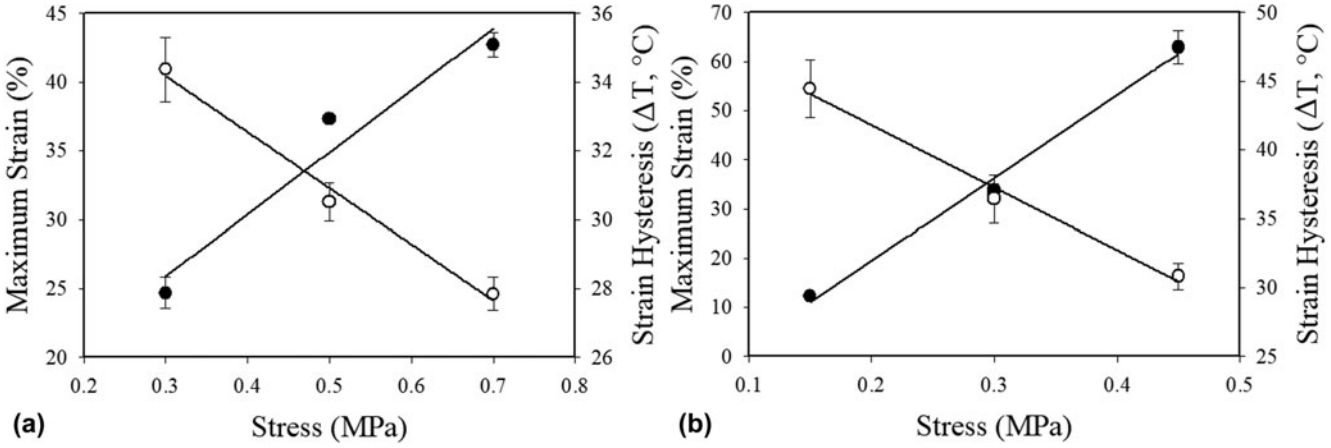


FIG. 7. Maximum strain and strain hysteresis versus stress based on the two-way shape memory behavior of (a) crosslinked cast film and (b) crosslinked spun fiber mat, respectively. Maximum strain (●) and strain hysteresis (○). The strain hysteresis was calculated from the temperature difference (ΔT) at the half of strain loop in two-way shape memory cycles.

constrained the degradation progress to varying extents that depend on the microstructural properties of the specific sample. Furthermore, water uptake experiments were done and found to support our interpretation of different degradation behaviors for each sample type (See the Supplementary Material, Fig. S2). Considering molecular weight evolution during enzymatic degradation, GPC tests [Fig. 8(c)] suggested that bulk degradation[47] was occurring over the duration of the study for both virgin film and virgin fiber mat, consistent to the results from previous work.[30] Moreover, we found no obvious shrinkage for both samples by examining the sizes visually (See the Supplementary Material, Fig. S3). On the other hand, the decreasing gel fraction during degradation [Fig. 8(d)] suggests bulk degradation for crosslinked cast films and fiber mats.

Although sharing similar tendency of the enzymatic degradation, all four types of samples behaved differently from each other upon closer inspection. Among the four types of samples, the crosslinked film underwent degradation at the lowest rate, which we attribute to its highest crystallinity. Unexpectedly, the crosslinked spun fiber mat exhibited a slower degradation rate than the crosslinked cast film, despite being processed by the same compression molding process that would ordinarily eliminate a structural difference. However, as we showed previously in SEM images, the crosslinked fiber mat in fact possessed a porous structure, potentially allowing more enzyme permeation into the films and reaction at internal surfaces within the pores. We determined that the density of the crosslinked film (~1.19 g/cm^3) was approximately 45% higher than that of the crosslinked fiber mat (~0.82 g/cm^3) (See the Supplementary Material, Table SII). Out of these four types of samples, only virgin fiber mat achieved complete degradation within our experimental time span. We attribute this mainly to the larger surface-to-volume ratio due to the highly porous structure, resulting in a larger contact area for lipases with polymers.

The effect of the enzymatic degradation on the surface morphology was studied for four different types of PCL_{3k}-TPU samples, respectively, using SEM (See the Supplementary Material, Fig. S4). For each type, the degraded samples at different select time points were compared to the control sample that was not treated with any PBS buffer. We observed that all the samples, except virgin fiber mat, revealed uniform rough surface after being exposed to enzymes, implying a lipase-specific erosion that is mediated by a surface-limited mechanism.[48] As with gradual increase of surface roughness associated with erosion degree, more and larger spherical pores could be found on the surface, especially in the later period of the study. These porous structures showed up starting at day 2 for the virgin film, but not until day 18 for the crosslinked film, in rough agreement with the degradation profiles of Fig. 8. For the crosslinked fiber mat, the original surface morphology disappeared almost completely within 2 d in the course of degradation, leaving an extremely rough surface. This phenomenon could be attributed to the unique, nonuniform internal structure [Figs. 2(d) and 2(h)]. Specifically, we postulate that the porosity was relatively higher on the surface versus at the center, and thereof, the sample began degrading in a similar way like the films did, once the surface layer has been degraded away relatively quickly. Different from the other three, the virgin fiber mat exhibited a characteristic "melted" structure where the fine, smooth fibers became relatively fluffy and swelled due to some bulk degradation.

https://doi.org/10.1557/jmr.2018.220 Published online by Cambridge University Press

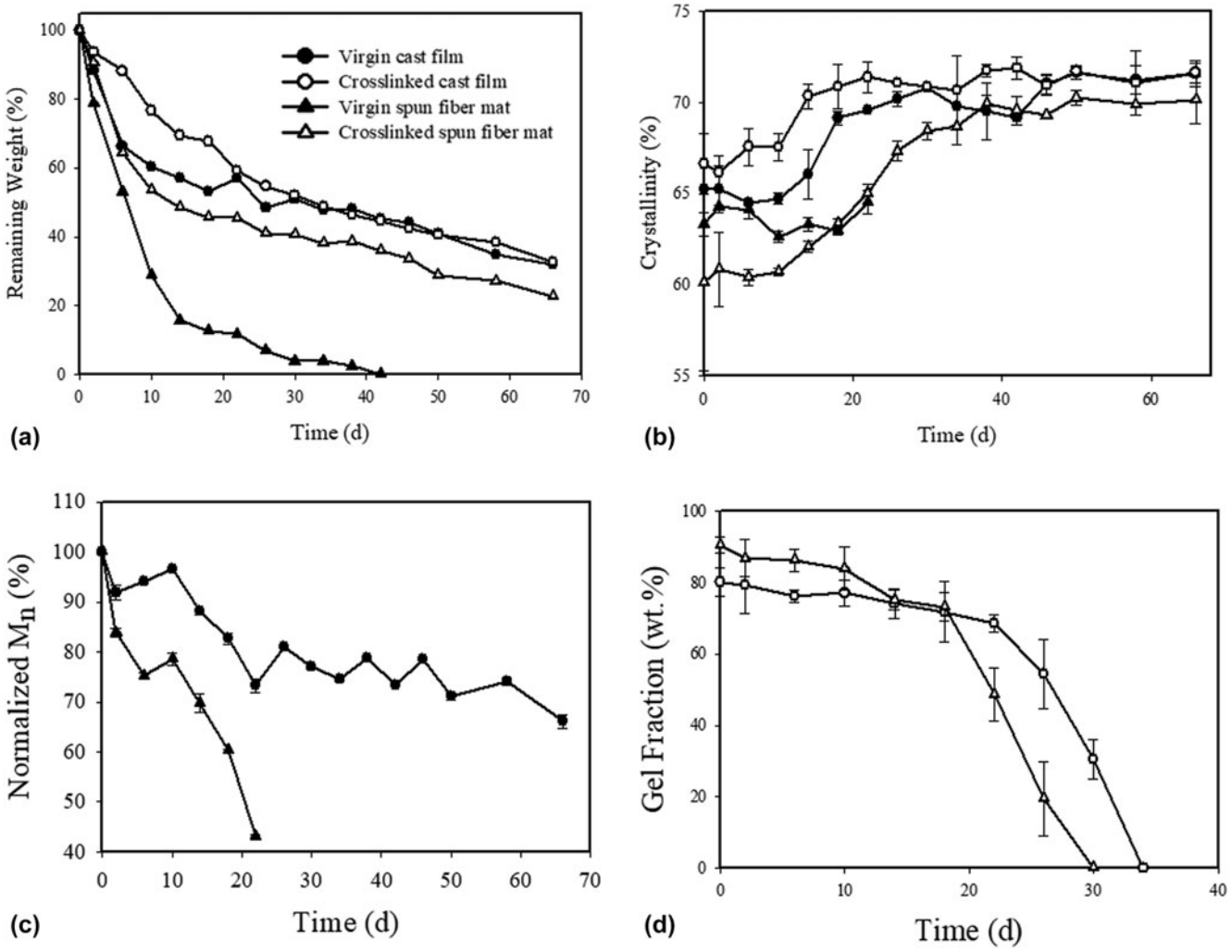


FIG. 8. Enzymatic degradation study of PCL_{3k}-TPU: (a) Mass remaining profiles, (b) crystallinities profiles, (c) normalized number-average molecular weight (M_n) remaining profiles for virgin samples only, and (d) evolution profiles of gel fraction value for crosslinked samples only during degradation by Lipase PS (0.4 mg/mL) in a pH 7.4 PBS solution at 37 °C. Virgin cast film (●), crosslinked cast film (○), virgin spun fiber mat (▲), and crosslinked spun fiber mat (△).

IV. CONCLUSIONS

Novel, versatile thermoplastic polyurethanes containing pendent unsaturation were prepared from a biodegradable soft segment, polycaprolactone-diol (PCL-diol), and a small functional diol with pendant allyl group, 3,4-dihydroxy-1-butene (DHB), and a diisocyanate using a one-pot synthesis technique. The molecular and thermal properties of these materials were investigated by GPC, DSC, and ^{1}H NMR initially, and PCL_{3k}-TPU was picked out for further study due to a suitable melting temperature that would allow favorable shape fixing. In this work, PCL_{3k}-TPU was successfully processed into films, by solvent casting and fiber mats, by electrospinning, respectively. Dilauroyl peroxide (DLP) was used as a thermal initiator to the crosslink film and spun mat samples covalently via the compression molding process. SEM images indicate successful formation of fiber at a scale of nanometers, and a unique structure containing partially melted fibers and homogeneously distributed phase. Analysis with a DMA illustrated that crosslinked PCL_{3k}-TPUs, either in a form of film or spun mat, exhibited outstanding one-way and two-way shape memory behaviors, both with good shape fixing and recovery. Furthermore, the critical stresses were estimated, indicating that crosslinked PCL_{3k}-TPUs needed no or very little stress for crystallization-induced elongation to be initiated, though increasing stress yielded proportionally increasing shape actuation.

An enzymatic degradation study revealed that the processing of samples resulted in quite different microstructures, playing a significant role in degradation behavior. We observed that the new PCL_{3k}-TPUs underwent bulk degradation in a two-step way that the degradation progressed faster in the first few days than

https://doi.org/10.1557/jmr.2018.220 Published online by Cambridge University Press

after. Considering the easy processability, exceptional reversible actuation, and predictable biodegradability, we envision that this family of latent-crosslinkable, biodegradable polyurethanes can be utilized in mechanical and medical applications including reversible actuators, sensors, and stents.

ACKNOWLEDGMENT

We gratefully acknowledge the funding for this work under NSF EFRI-1435452.

REFERENCES

1. A. Lendlein and S. Kelch: Shape memory polymers. *Angew. Chem., Int. Ed.* **41**, 2034 (2002).
2. D. Ratna and J. Karger-Kocsis: Recent advances in shape memory polymers and composite: A review. *J. Mater. Sci.* **43**, 254 (2008).
3. C. Liu, H. Qin, and P.T. Mather: Review of progress in shape memory polymers. *J. Mater. Chem.* **17**, 1543 (2007).
4. T. Xie: Tunable polymer multi-shape memory effect. *Nature* **464**, 267 (2010).
5. K. Yu, T. Xie, J. Leng, Y. Ding, and H.J. Qi: Mechanisms of multi-shape memory effects and associated energy release in shape memory polymers. *Soft Matter* **8**, 5687 (2012).
6. P.T. Mather, X. Luo, and I.A. Rousseau: Shape memory polymer research. *Annu. Rev. Mater. Res.* **39**, 445 (2009).
7. J. Li, W.R. Rodgers, and T. Xie: Semi-crystalline two-way shape memory elastomer. *Polymer* **52**, 5320 (2011).
8. K.K. Westbrook, P.T. Mather, V. Parakh, M.L. Dunn, Q. Qi, B.M. Lee, and H.J. Qi: Two-way reversible shape memory effects in a free-standing polymer composite. *Smart Mater. Struct.* **20**, 065010 (2011).
9. D.K. Shenoy, D.L. Thomsen, III, A. Srinivasan, P. Keller, and B.R. Ratna: Carbon coated liquid crystal elastomer film for artificial muscle applications. *Sens. Actuators, A* **96**, 184 (2002).
10. J. Leng, X. Lan, Y. Liu, and S. Du: Shape memory polymers and their composites: Stimulus methods and applications. *Prog. Mater. Sci.* **56**, 1077 (2011).
11. Y. Yu and T. Ikeda: Soft actuators based on liquid-crystalline elastomers. *Angew. Chem., Int. Ed.* **45**, 5416 (2006).
12. C. Ohm, M. Brehmer, and R. Zentel: Liquid crystalline elastomers as actuators and sensors. *Adv. Mater.* **22**, 3366 (2010).
13. S. Krause, F. Zander, G. Bergmann, H. Brandt, H. Wertmer, and H. Finkelmann: Nematic main-chain elastomers: Coupling and orientational behavior. *C. R. Chim.* **12**, 85 (2009).
14. T. Chung, A. Romo-Uribe, and P.T. Mather: Two-way reversible shape memory in a semicrystalline network. *Macromolecules* **41**, 184 (2008).
15. R.M. Baker, J.H. Henderson, and P.T. Mather: Shape memory poly(ε-caprolactone)-*co*-poly(ethylene glycol) foams with body temperature triggering and two-way actuation. *J. Mater. Chem. B* **1**, 4916 (2013).
16. M. Behl, K. Kratz, J. Zotzmann, U. Nőchel, and A. Lendlein: Reversible bidirectional shape memory polymers. *Adv. Mater.* **25**, 4466 (2013).
17. J. Zhou, S.A. Turner, S.M. Brosnan, Q. Li, J.Y. Carrilo, D. Nykypanchuk, O. Gang, V.S. Ashby, A.V. Dobrynin, and S.S. Sheiko: Shape-shifting: Reversible shape memory in semicrystalline elastomers. *Macromolecules* **47**, 1768 (2014).
18. N. Teramoto, H. Kogure, Y. Kimura, and M. Shibata: Thermal properties and biodegradability of the copolymers of L-lactide, ε-caprolactone, and ethylene glycol oligomer with maleate units and their crosslinked products. *Polymer* **45**, 7927 (2004).
19. P. Ping, W. Wang, X. Chen, and X. Jing: The influence of hard-segments on two-phase structure and shape memory properties of PCL-based segmented polyurethanes. *J. Polym. Sci., Part B: Polym. Phys.* **45**, 557 (2007).
20. B.K. Kim and S.Y. Lee: Polyurethanes having shape memory effects. *Polymer* **37**, 5781 (1996).
21. A.E. Senador, Jr., M.T. Shaw, and P.T. Mather: Electrospinning of polymeric nanofibers: Analysis of jet formation. *Mater. Res. Soc. Symp. Proc.* **661**, 5.9.1 (2001).
22. A. Greiner and J.H. Wendorff: Electrospinning: A fascinating method for the preparation of ultrathin fibers. *Angew. Chem., Int. Ed.* **46**, 5670 (2007).
23. M.M. Demir, I. Yilgor, E. Yilgor, and B. Erman: Electrospinning of polyurethane fibers. *Polymer* **43**, 3303 (2002).
24. G. Odian: *Principles of Polymerization*, 4th ed. (A John Wiley & Sons, Inc., New Jersey, 2004); p. 619.
25. O. Gǔven: *Crosslinking and Scission in Polymers* (Springer, Netherlands, 1990); p. 1.
26. P.C. Boire, M.K. Gupta, A.I.L. Zachman, S.H. Lee, D.A. Balikov, K. Kim, L.M. Bellan, and H. Sung: Pendant allyl crosslinking as a tunable shape memory actuator for vascular applications. *Acta Biomater.* **24**, 53 (2015).
27. M.I. Lawton, K.R. Tillman, H.S. Mohammed, W. Kuang, D.A. Shipp, and P.T. Mather: Anhydride-based reconfigurable shape memory elastomers. *ACS Macro Lett.* **5**, 203 (2016).
28. Z. Gan, Q. Liang, J. Zhang, and X. Jing: Enzymatic degradation of poly(ε-caprolactone) film in phosphate buffer solution containing lipases. *Polym. Degrad. Stab.* **56**, 209 (1997).
29. J. Zeng, X. Chen, Q. Liang, X. Xu, and X. Jing: Enzymatic degradation of poly(L-lactide) and poly(ε-caprolactone) electrospun fibers. *Macromol. Biosci.* **4**, 1118 (2004).
30. X. Gu, J. Wu, and P.T. Mather: Polyhedral oligomeric silsesquioxane (POSS) suppresses enzymatic degradation of PCL-based polyurethanes. *Biomacromolecules* **12**, 3066 (2011).
31. X. Luo and P.T. Mather: Preparation and characterization of shape memory elastomeric composites. *Macromolecules* **42**, 7251 (2009).
32. J.M. Robertson, H.B. Nejad, and P.T. Mather: Dual-spun shape memory elastomeric composites. *ACS Macro Lett.* **4**, 436 (2015).
33. K.A. Burke, I.A. Rousseau, and P.T. Mather: Reversible actuation in main-chain liquid crystalline elastomers with varying crosslink densities. *Polymer* **55**, 5897 (2014).
34. M.A. Rice, J. Samchez-Adams, and K.S. Anseth: Exogenously triggered, enzymatic degradation of photopolymerized hydrogels with polycaprolactone subunits: Experimental observation and modeling of mass loss behavior. *Biomacromolecules* **7**, 1968 (2006).
35. V.P. Saraf, W.G. Glasser, G.L. Wilkes, and J.E. McGrath: Structure-property relationships of PEG-containing polyurethane networks. *J. Appl. Polym. Sci.* **30**, 2207 (1985).
36. E. McMullin, H.T. Rebar, and P.T. Mather: Biodegradable thermoplastic elastomers incorporating POSS: Synthesis, microstructure, and mechanical properties. *Macromolecules* **49**, 3769 (2016).
37. A. Valério, D.S. Conti, P.H.H. Araújo, C. Sayer, and S.R.P. da Rocha: Synthesis of PEG-PCL-based polyurethane nanoparticles by miniemulsion polymerization. *Colloids Surf., B* **135**, 35 (2015).
38. B.S. Lee, B.C. Chun, Y.C. Chung, K.I. Sul, and J.W. Cho: Structure and thermomechanical properties of polyurethane block copolymers with shape memory effect. *Macromolecules* **34**, 6431 (2001).
39. M. Ahmad, B. Xu, H. Purnawali, Y. Fu, W. Huang, M. Miraftab, and J. Luo: High performance shape memory polyurethane synthesized with high molecular weight polyol as the soft segment. *Appl. Sci.* **2**, 535 (2012).

https://doi.org/10.1557/jmr.2018.220 Published online by Cambridge University Press

40. N. Barkoula, T. Peijs, T. Schimanski, and J. Loos: Processing of single polymer composites using the concept of constrained fibers. *Polym. Compos.* **26**, 114 (2005).
41. N.K. Kim, S. Fakirov, and D. Bhattacharyya: Polymer–polymer and single polymer composites involving nanofibrillar poly(vinylidene fluoride): Manufacturing and mechanical properties. *J. Macromol. Sci., Part B: Phys.* **53**, 1168 (2014).
42. S. Jiang, C. He, Y. Men, X. Chen, L. An, S.S. Funari, and C. Chan: Study of temperature dependence of crystallization transitions of a symmetric PEO–PCL diblock copolymer using simultaneous SAXS and WAXS measurements with synchrotron radiation. *Eur. Phys. J. E: Soft Matter Biol. Phys.* **27**, 357 (2008).
43. M. Krumova, D. López, R. Benavente, C. Mijangos, and J.M. Pereña: Effect of crosslinking on the mechanical and thermal properties of poly(vinyl alcohol). *Polymer* **41**, 9265 (2000).
44. J. Park, Q. Ye, E.M. Topp, C.H. Lee, E.L. Kostoryz, A. Misra, and P. Spencer: Dynamic mechanical analysis and esterase degradation of dentin adhesives containing a branched methacrylate. *J. Biomed. Mater. Res., Part B* **91**, 61 (2009).
45. L. Song, Q. Ye, X. Ge, A. Misra, J.S. Laurence, C.L. Berrie, and P. Spencer: Synthesis and evaluation of novel dental monomer with branched carboxyl acid group. *J. Biomed. Mater. Res., Part B* **102**, 1473 (2014).
46. C. Liu, S.B. Chun, and P.T. Mather: Chemically cross-linked polycyclooctene: Synthesis, characterization, and shape memory behavior. *Macromolecules* **35**, 9868 (2002).
47. L.S. Nair and C.T. Laurencin: Biodegradable polymers as biomaterials. *Prog. Polym. Sci.* **32**, 762 (2007).
48. E.M. Christenson, S. Patel, J.M. Anderson, and A. Hiltner: Enzymatic degradation of poly(ether urethane) and poly(carbonate urethane) by cholesterol esterase. *Biomaterials* **27**, 3920 (2006).

Supplementary Material

To view supplementary material for this article, please visit https://doi.org/10.1557/jmr.2018.220.

https://doi.org/10.1557/jmr.2018.220 Published online by Cambridge University Press